Hindawi
Shock and Vibration
Volume 2022, Article ID 3679431, 16 pages
https://doi.org/10.1155/2022/3679431

Research Article

Experimental and Numerical Investigation on Seismic Performance of RC Exterior Beam-Column Joints with Slabs

Zhimeng Wang, Jiao Huang, Zhaoqun Chang, and Yongjian Lu

School of Civil Engineering, Chang'an University, Xi'an 710061, China

Correspondence should be addressed to Zhimeng Wang; 2018028006@chd.edu.cn

Received 30 June 2022; Revised 25 August 2022; Accepted 2 September 2022; Published 19 September 2022

Academic Editor: Yonggang Zhang

The effect of a cast-in-place slab on the beam-column joint at beam ends in reinforced concrete (RC) structures under earthquake attacks has not been fully understood, and therefore, it is not manifestly addressed to some of the design criteria or specifications. Consequently, the contribution of slab to the seismic resistance of structures is often ignored or just included in an approximate manner. In this study, the experiment of two 1/2-scaled exterior beam-column joints without slabs and three 1/2-scaled joints with slabs under the combination of quasi-static repeated cyclic loading and constant axial force was carried out to investigate the effect of the cast-in-place slab on the seismic performance of exterior beam-column joints. The results show that for specimens EBCJ1 and EBCJ2 without slab, the decline was approximately 5%, while for specimens EBCSJ1 and EBCSJ3, the decline in the load is obvious and approximately more than 10%. For specimen EBCSJ2, which exhibited a slightly different behavior in the hysteresis curves, the maximum carrying capacity reached at the displacement of 70 mm during the first cycle. The cast-in-place slab has different effects on the failure mechanism and load transfer mechanism of the exterior beam-column joint, which depends on the column-beam moment strength ratio in the loading protocol. The slab has a positive effect on the energy dissipation capacity of the joint but has a negative effect on the load carrying capacity. In addition, finite element (FE) analysis of the tested specimens was conducted. The FE numerical models were established based on the construction information and loading conditions from the experiment and then validated by comparing them with the experimental observation.

1. Introduction

The research on the seismic behavior of RC frame structures has always been a hot topic in the field of civil engineering. Beam-column joint subassembly element consists of the component beam, column, and joint, which is a local characterization of RC frame and can be considered to have the same response as the frame under earthquake. Experimental results and actual cases showed that the damage of the RC frame structure under postearthquake was mainly localized at the beam-column joints, which may contribute to partial or complete collapse of the structure [1–3].

Considering that the exterior beam-column joints play an important role in maintaining the integrity of the whole RC frame structures, extensive studies on the seismic performance of exterior beam-column joints have been performed [4–12]. Alva et al. [13] studied the influence of joint transverse reinforcement ratio and concrete compressive strength on the performance of the joint specimens through the test of four exterior RC beam-column joints under reversal cyclic loading. The test results show that the concrete compressive strength is the primary factor affecting the joint shear capacity. The transverse reinforcement of joints also has a certain influence on the load-displacement response of such joints. Sasmal et al. [14] designed exterior beam-column joints according to the provisions of Eurocode and Indian Standards and evaluated the seismic behavior of the joints. Test results show that the exterior beam-column joints based on Eurocode and Indian Standards have almost similar performance in stiffness and strength degradation. Nevertheless, the specimens designed according to the Indian Standards represent higher energy dissipation at a preset drift ratio. Marthong et al. [15] studied the influence of different frequencies' cyclic excitations on the seismic

behavior of external RC beam-column specimens with typical deficiencies. The results indicate that the influencing effect of the loading rate is significant in beam-column joints with beam weak in flexure, while the effect is not so significant in the other joints. Karayannis et al. [16, 17] conducted an experiment on full-scale exterior beam-column connection subassemblages and used carbon fiber ropes as external strengthening reinforcement to increase the seismic capacity of the test specimens.

In previous studies of beam-column joints, it was found that the slab has a significant impact on the seismic performance of the joints. The results of the study indicate that the presence of slabs affects the behavior of the joint in two ways [18–21]. One is that it increases the flexural strength of the beam, thus decreasing the moment strength ratio. Second, it increases the shear bearing capacity of the joint. However, for an exterior beam-column joint with slab, the damage mode and mechanism of the joint are not clear under earthquake action. Further research is needed to be carried out to give a deep understanding on this issue.

A few scholars have studied the effect of slabs on the force performance of exterior beam-column joint under earthquake action. Kam et al. [22] tested four corner beam-column joints with floor slab under low reversed lateral loading and axial compressive forces. The test results show the very poor seismic performance of the joints, characterized by a severe loss of stiffness, with extrusion and strength loss starting in the early stages of loading. Park and Mosalam [23] carried out an experimental study on four corner beam-column joints with slabs. Their investigation focused on the influence of some key parameters on the shear strength and deformability of external joints, and the test results were compared to the ASCE 41 recommendations. However, the parameters affecting joint shear damage were not adequately evaluated numerically in these studies. French and Moehle [24] counted the experimental results of 13 interior beam-column joints and 7 exterior beam-column joints, and it was found that the calculated load capacity without considering the slab was 25% and 17% lower than the measured load capacity considering the action of the slab, respectively. Furthermore, several researchers have tested beam-column joints to better understand the resistance and failure mechanics of the beam-column joint by taking the slab into account and trying to modify the design specifications to account for the effect of slab [25–30].

The few existing studies on exterior beam-column with slab have shown that slab has a significant influence on the force performance of the joints; however, these studies either represent corner joints [22, 23] or include significant connection reinforcement in seismic design. Most studies do not have a very clear description of the mechanism of slab to joint action. Moreover, there is a lack of numerical models to realistically simulate the mechanism of slab action in exterior beam-column joints. Therefore, it is necessary to further investigate the exterior beam-column joints with slab.

Based on the current deficiencies, to study the contribution of the slab in the beam-column joint and the mechanism of its action on the joints, the experimental investigation on five exterior beam-column joints with or without slabs was performed. The specimens were loaded in a cyclic loading system to simulate the seismic response of the beam-column joints under earthquake loads. The effect of slab on the shear demand of the beam-column joint was determined by inspecting the slab strain. The deformability in terms of the drift ratios of these joints was mainly analyzed. In addition, FE analysis was conducted to numerically simulate the behavior of exterior beam-column joint under earthquake action, and the results were compared to that from experiment to validate the feasibility and accuracy of the FE analysis model. In this study, the relevant experimental analysis and finite element simulation of exterior beam-column joints with or without slabs are carried out based on the experimental results of Xing et al. [31].

2. Experimental Program

2.1. Specimen Details and Primary Variables. In this experiment, five half-scale RC exterior beam-column joints were designed and constructed, according to Chinese code for seismic design of buildings (GB50011-2010) [32]. Then, the specimens were tested under quasi-static repeated cyclic loading and combination of constant axial force to investigate the seismic behavior. Figure 1 illustrates the dimensions of the reference specimen and details of the arrangement of steel reinforcements. Except for the design parameters that consist of the slab and the moment strength ratio of column to beam, all specimens had the same construction details for the joints. As shown in Figure 1, the length of the column was 1950 mm with a square cross section of 250 mm × 250 mm. The length of longitudinal beam from the column surface to the free beam end was 1750 mm, with a rectangular section of 150 mm × 280 mm.

The reinforcement details of the exterior beam-column joints are given in Figure 1. All specimens were denoted with four characters: "E" for exterior, "B" for the longitudinal beam, "C" for column, "S" for slab, and "J" for joint. As shown in Table 1, all the specimens have the same reinforcement details for the beams in the joints. The configuration of stirrups is in accordance with the relevant Chinese codes [32] for minimum reinforcement requirement. Specimens EBCJ1 and EBCJ2 are beam-column joints without slab, and specimens EBCSJ1, EBCSJ2, and EBCSJ3 are beam-column joints with slab. The effect of slab on the seismic performance of the joints is investigated through the experimental study of joints with or without slab. The width of the slab was 1750 mm with the thickness of 60 mm.

2.2. Material Properties. The joint specimens in this study were fabricated using the ready-mixed concrete, which had an average compressive strength of 24.3 MPa obtained from three 150 mm cubes. Direct tensile tests of five reinforcement samples were carried out to obtain the mechanical properties of the steel reinforcements employed in this study. Table 2 lists the average test results of the mechanical properties of three coupon samples for each diameter of the

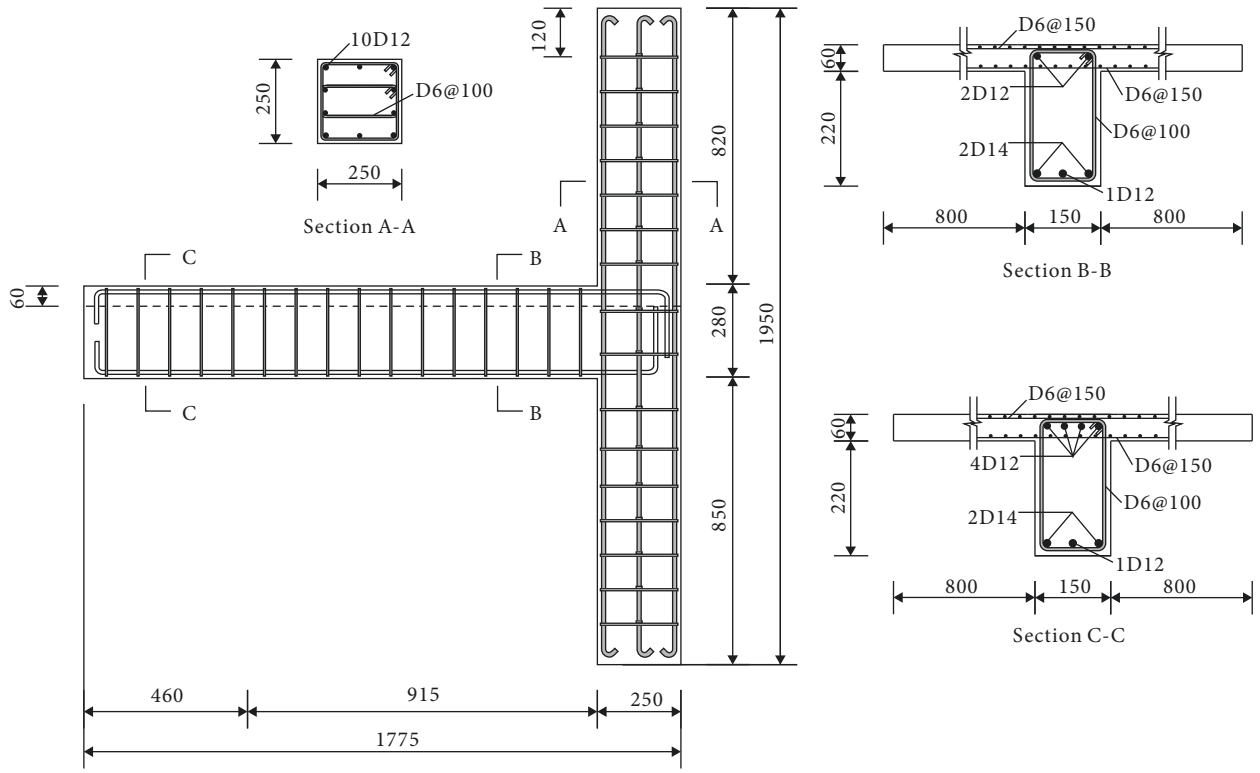

Figure 1: Details of the reinforcement layout in the specimens (dimensions are in mm; D = diameter of the deformed bar).

Table 1: Main design parameters and important values.

	Specimen	EBCJ1	EBCJ2	EBCSJ1	EBCSJ2	EBCSJ3
Beam	Section (mm×mm)	150 × 280	150 × 280	150 × 280	150 × 280	150 × 280
	Top reinforcing bars	2D12	2D12	2D12	2D12	2D12
	Bottom reinforcing bars	2D14 + 1D12	2D14 + 1D12	2D14 + 1D12	2D14 + 1D12	2D14 + 1D12
	Stirrup	D6@100	D6@100	D6@100	D6@100	D6@100
Column	Section (mm×mm)	250 × 250	250 × 250	250 × 250	250 × 250	280 × 280
	Reinforcing bars	2 × 4D12	2D14 + 2D12	2 × 4D12	2D14 + 2D12	2D16 + 2D14
	Stirrup	D6@100	D6@100	D6@100	D6@100	D8@100
Slab	Thickness (mm)	None	None	60	60	60
	Longitudinal direction	None	None	D6@150	D6@150	D6@150
	Transverse direction	None	None	D6@150	D6@150	D6@150
Joint	Stirrup	D6@100	D6@100	D6@100	D6@100	D8@100
	Ratio, ρ_v (%)	0.45	0.45	0.45	0.45	0.72
Axial compressive force (kN)		230	230	230	230	295

Table 2: Material properties of steel reinforcements.

Diameter (mm)	6	8	10	12	14
Yield strength (MPa)	401.2	441.1	446.1	455.2	432.1
Yield strain ($\times 10^{-6}$)	1924	2139	2443	2226	2369
Ultimate strength (MPa)	571.6	558.7	650.7	601.7	610.9

reinforcement, including the yield and ultimate strength, yield strain, and the modulus of elasticity.

2.3. Test Setup. The overview of the test setup for the exterior beam-column joints is presented in Figure 2. The specimens were tested under quasi-static cyclic loading at the column top to simulate the earthquake effect. Meanwhile, the constant vertical axial load of 295 kN was applied on the surface of the column top for specimen EBCSJ3 and 230 kN for the other joint specimens. Both the lateral loads and vertical axial loads were applied by a 500 kN hydraulic actuator. To simulate the response of the joint in an actual frame structure, one of the ends of the beam and the column was pinned. For the beam, the free end was pinned by a vertical steel link, as shown in Figure 2, to restrain the

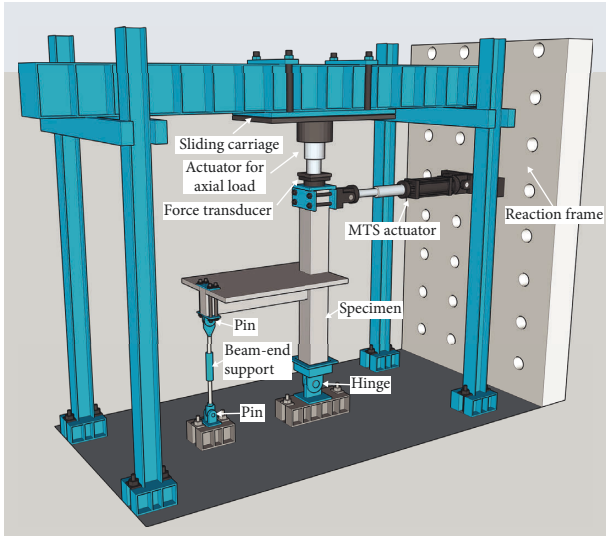

Figure 2: Test setup.

vertical movement at the beam end. The pin for the column was installed at the base of the column to avoid any deformation at this point, and only lateral deflection was allowed at the top of the column.

During the test, the loads and the lateral displacements of the column top were recorded by the hydraulic actuator. To measure the shear deformations at the core area of the exterior beam-column joints, two displacement transducers were installed at the core area in the diagonal directions. Then, the shear deformation was determined by converting the relative displacement obtained by the two displacement transducers. In addition to the displacements, the strains of steel reinforcements in beams and columns were collected by strain gauges, as well as the strains in the joint region and slabs. The strain gauges had the length of 3 mm and were installed on the longitudinal steel bars and in beams/columns and the transverse reinforcements in the joint region, as well as on the distributed reinforcements in slabs. Figure 3 shows typical locations of the strain gauges on the longitudinal and transverse reinforcements in the beam and the column.

2.4. Loading Sequences. For the exterior beam-column joints, axial compression load was applied on the column top one day prior to the test in order to eliminate any immediate creep effect. Afterwards, the axial compression loads were kept constant throughout the test, while cyclic lateral loads were applied by hydraulic actuator in displacement control system. In this test, two typical displacement sequences were adopted as shown in Figure 4, which refers to the Chinese code (specification for seismic test of buildings (JGJ/T 101–2015)) [33]. Before the specimens' yield, the loading scheme involved one push-pull cycle with a horizontal displacement increasing by 5 mm at each step. Then, the quasi-static application of displacement increased by a half of the yield displacement and was repeated for three cycles for each step. To utilize results obtained from static cyclic loading tests on structural elements or large subassemblages for a general performance evaluation, there is the need to establish loading history that captures the critical issues of the subassemblage capacity and the seismic demands. For specimens EBCJ1, EBCJ2, and EBCSJ2, the amplitude of the applied displacements at the column top was increased from 0 mm to 20 mm with a step of 5 mm and then increased with the step of 10 mm up to failure. When the displacement was less than 10 mm, only one cycle was applied for each step. After reaching more than 10 mm of displacement at the top of the column, the load was repeated three times in each step. For specimens EBCSJ1 and EBCSJ3, the loading step of the applied displacements was the same with the former three specimens before reaching 20 mm. After that, the loading step was increased to 20 mm. The applied displacement was also repeated one time a step before 10 mm was reached and increased to three times a step after reaching 10 mm. As shown in Figure 4, specimens EBCJ1, EBCJ2, EBCSJ4, and EBCSJ2 would experience more repeated cyclic lateral loads than specimens EBCSJ1 and EBCSJ3. Generally, 26 cycles and 17 cycles of displacement loading were planned for the former three joint specimens and the latter two specimens, respectively, with the maximum story drift ratio of 4.1%. In actual experiments, when the bearing capacity of the beam-column joint dropped to about 80% of the peak load capacity, the test is stopped.

3. Experimental Results and Discussion

The experimental results of the exterior beam-column joints under quasi-static cyclic lateral loading were presented and systematically analyzed in terms of (1) overall behavior, (2) load versus displacement hysteretic curves, and (3) analytical evaluation of slab effect.

3.1. Overall Behavior. In the experiment, the overall behavior of the test specimens regarding the crack initiation and propagation was mainly recorded as closely as possible. The failure modes attached with a close view of the joint core region for all the specimens are illustrated in Figure 5. Note that crushing of concrete was observed in all the specimens started from the beam-column joint region and then was extended up to the joint core area.

As shown in Figures 5(a) and 5(b), for specimens EBCJ1 and EBCJ2 without slab, it can be observed that the flexural cracks alternately appeared in the upper and lower parts of the front of the beam adjacent to the column surface under the repeated cyclic lateral loading. When the column reached the drift ratio of 1.5%, the flexural cracks penetrated across the full length of the beam height. In addition, diagonal crack emerged at the core of the joints once the diagonal tensile stress increases and passes the ultimate tensile strength of the concrete. Then, the shear cracks propagate and expand as the displacement is applied continuously. At drift ratios between 2% and 3%, the initial sign of shear failure of the joints could be observed due to the considerable expansion of these shear cracks. From Figure 5(a), severe crushing of concrete at the face of the column was found in specimen EBCJ1 when failed. The plastic hinge was not formed in EBCJ1 as there was no

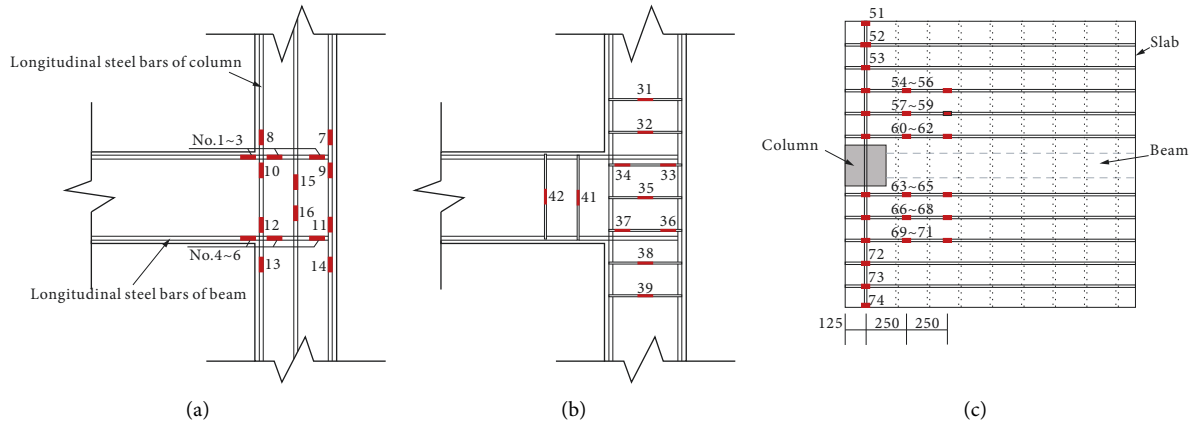

Figure 3: Arrangement of strain gauges for steel bars. (a) Strain gauges of longitudinal reinforcement. (b) Strain gauges of stirrup. (c) Strain gauges of steel reinforcement in slab.

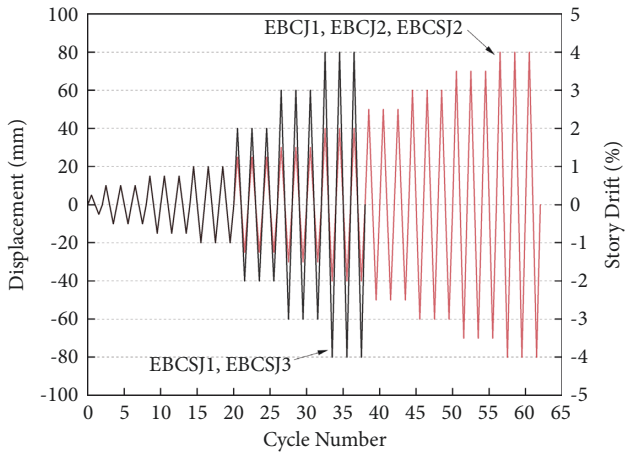

Figure 4: Cyclic loading history.

obvious damage on the beam surface except for the visible cracks. While for specimen EBCJ2 with higher flexural strength ratio of column to beam than EBCJ1, as expected, plastic hinge is formed at the beam end close to the column juncture, which caused serious damage of the beams.

For specimens EBCSJ1, EBCSJ2, and EBCSJ3 with cast-in-place slabs existing, as shown in Figures 5(c)~5(e), flexural cracks with uniform distribution were observed mainly at the lower part of the front of the beam. Affected by the existence of the slab, few flexural cracks occurred in the upper part of the beam. On the other hand, compared with the specimens without slab, the three joints present a more serious damage at the core area of the joints, showing fully developed criss-cross diagonal shear cracks here. Besides, torsional cracks of beam-column joints with slab generally emerged in the second loading cycle. These torsional cracks started on the back of the slabs near the column and inclined at an angle of approximately 37°. Similarly, when the drift ratio reached 2%, flexural cracks were fully formed upward to the top of the beam. When the column reached to 3% drift ratio, the shear cracks on the joint widened and presented the signal of joint shear failure.

Since cracked, the cracks on the concrete progressively propagated as the load increased; meanwhile, new cracks initiated constantly. For beam-column joints, a crack width of 0.3 mm is set for "critical crack." When the width of a pair of large diagonal cracks is more than 0.3 mm, it can be considered that the stirrup in the core area of the joint started to yield, and the specimen reaches its maximum load carrying capacity as the load would increase within a limited range, as well as the ultimate shear strength. However, in this condition, the shear deformation in the core region of the joint would be significantly increased since the stiffness of the joint specimen had decreased severely. When the specimen failed, crushing of concrete at the joint core could be observed, which would lead to a notable drop loss in the load bearing capacity of the joint. Finally, the test would be stopped when the decrease in the load exceeds 20% of the ultimate strength.

3.2. Load versus Displacement Hysteretic Curves. As shown in Figure 6, typical spindle hysteresis loops can be observed for specimens EBCJ1, EBCJ2, EBCSJ1, and EBCSJ3, while specimen EBCSJ2 exhibited a narrower shape in the load-displacement hysteresis curves. In the early loading stage, as the applied displacement was less than 10 mm, the hysteresis loops were as narrow as a small strip. When unloading load, the deformation of the specimens could return to its initial position, and the area surrounded by the hysteresis loops was small. When the applied displacements increased to 20 mm, unrecoverable deformation could be observed in the hysteresis curves, indicating the occurrence of plastic deformation of the specimens. At this point, the slope of the specimens had not decreased. After the displacement reaches 40 mm, the specimen load carrying capacity was increased slowly as the displacement continued to be applied. Moreover, with the increase in the loading cycle, the carrying capacity of the specimens decreased greatly, resulting in a significant decrease in the areas surrounded by the hysteresis loops. When the displacements reached 60 mm, except for EBCSJ2, all the specimens reached their maximum load carrying capacity at the first cycle. From the figure, a considerable decline in the loads was observed during the second cycle of loading, and

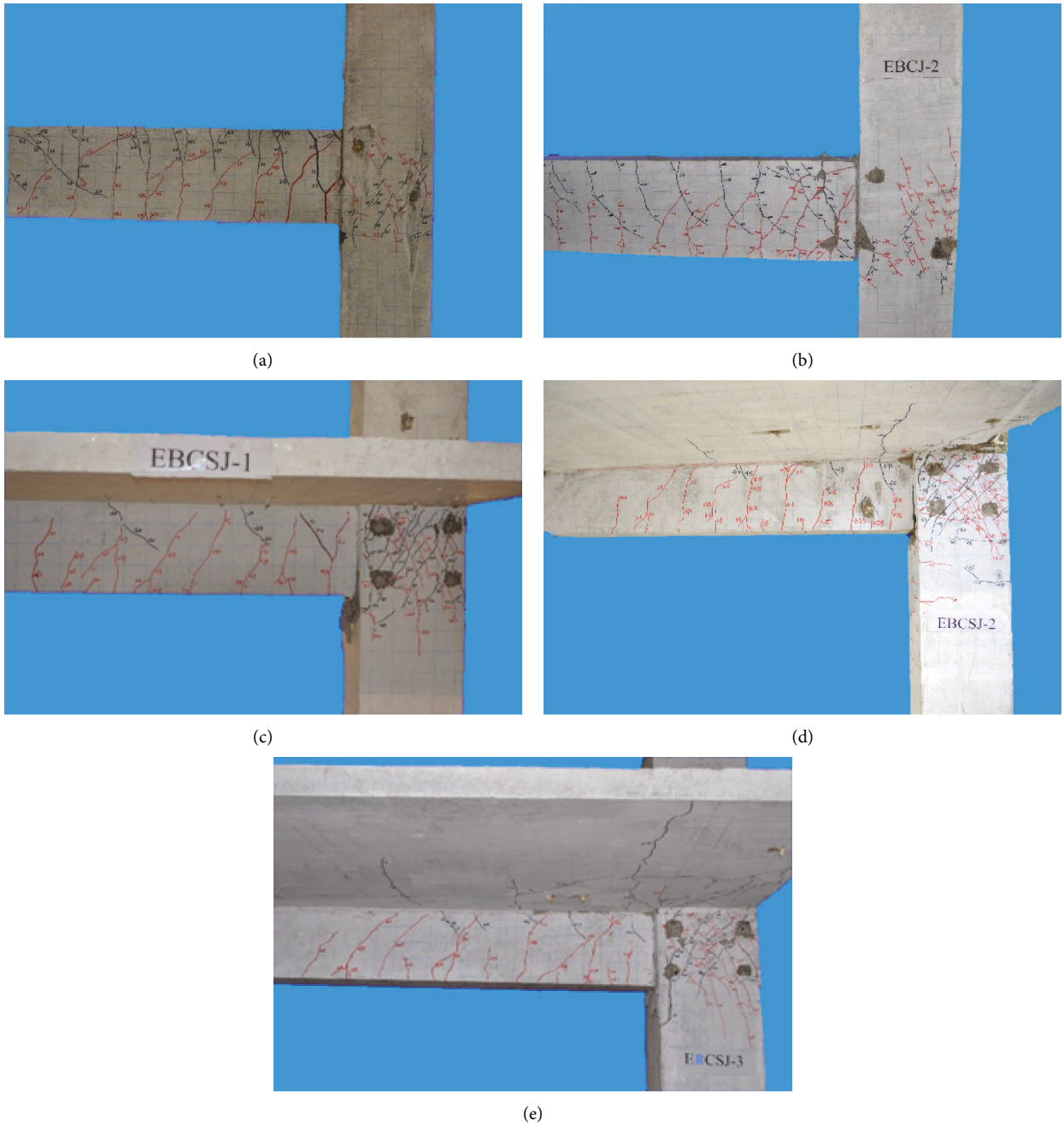

Figure 5: Failure mode of exterior joints. (a) EBCJ1. (b) EBCJ2. (c) EBCSJ1. (d) EBCSJ2. (e) EBCSJ3.

smaller decline occurred at the third cycle. For specimens EBCJ1 and EBCJ2 without slab, the decline was approximately 5%, while for specimens EBCSJ1 and EBCSJ3, the decline in the load is obvious and approximately more than 10%. For specimen EBCSJ2, which exhibited a slightly different behavior in the hysteresis curves, the maximum carrying capacity reached at the displacement of 70 mm during the first cycle.

3.3. Analytical Evaluation of Slab Effect. Figure 7 shows the strain variation of slab top reinforcement obtained from the bonded strain gauges (in Figure 3). Experimental results show that the strain value decreases as the distance from the column face. This shows the effect of slab reinforcements on the negative moment bearing capacity of longitudinal beams. For the three specimens, the strains in all the longitudinal reinforcements were increased as displacements were applied, indicating the increased participation of the slabs to the beam moment strengths and joint shear demands. The slab bar nearest to the beam generally experienced the largest increase in strain. The results show that the slab contribution could effectively enhance the negative moment at the beam. This is because the longitudinal reinforcement in the slabs is used as the tensile reinforcement

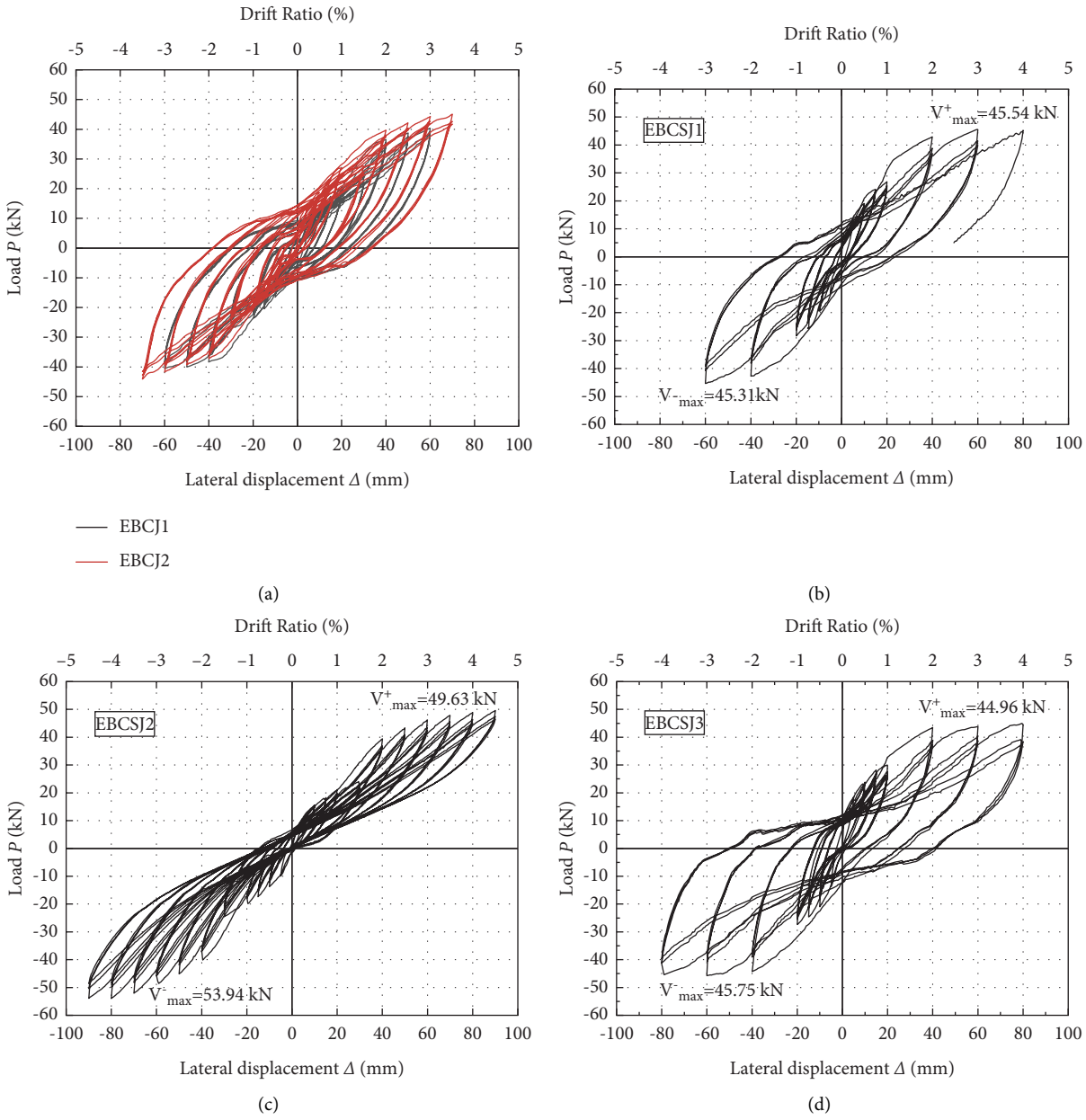

Figure 6: Load versus displacement hysteretic curves. (a) EBCJ1, EBCJ2. (b) EBCSJ1. (c) EBCSJ2. (d) EBCSJ3.

of the beams. Therefore, with more slab reinforcement participating in the larger deformation demand, the tensile reinforcement in the beam increases effectively with the increase in curvature.

As shown in Figure 8, it shows the crack development of the slab on each joint during the loading process. We can see from the figure that the development of cracks in the three specimens during the loading process is basically similar, the cracks are mostly developed on the slab in the column width area, and the cracks are distributed throughout the length of the beam body. It can be seen from the damage morphology that the slab on the beam retards the appearance of cracks on the beam under the horizontal load and reduces the damage of the beam. In addition, the comparison shows that the damage of specimen EBCSJ2 is more serious, and serious concrete stripping occurred at the intersection of column and slab; thus, it can be seen that the loading regime has serious influence on the joints with slab.

3.4. Behavior of Hoops in Joint Core. The function of the stirrups in the core area is to constrain the concrete in the core area to improve the shear bearing capacity of the core area. The arrangement of the stirrup measuring points of each specimen in this test is shown in Figure 3. During the experiment, the position of the core area of each specimen and the strain values of the stirrups nearby were recorded, and the influence of the plate on the seismic performance of the joint was further analyzed through the strain changes in these stirrups. The distribution of stirrup strain in the core

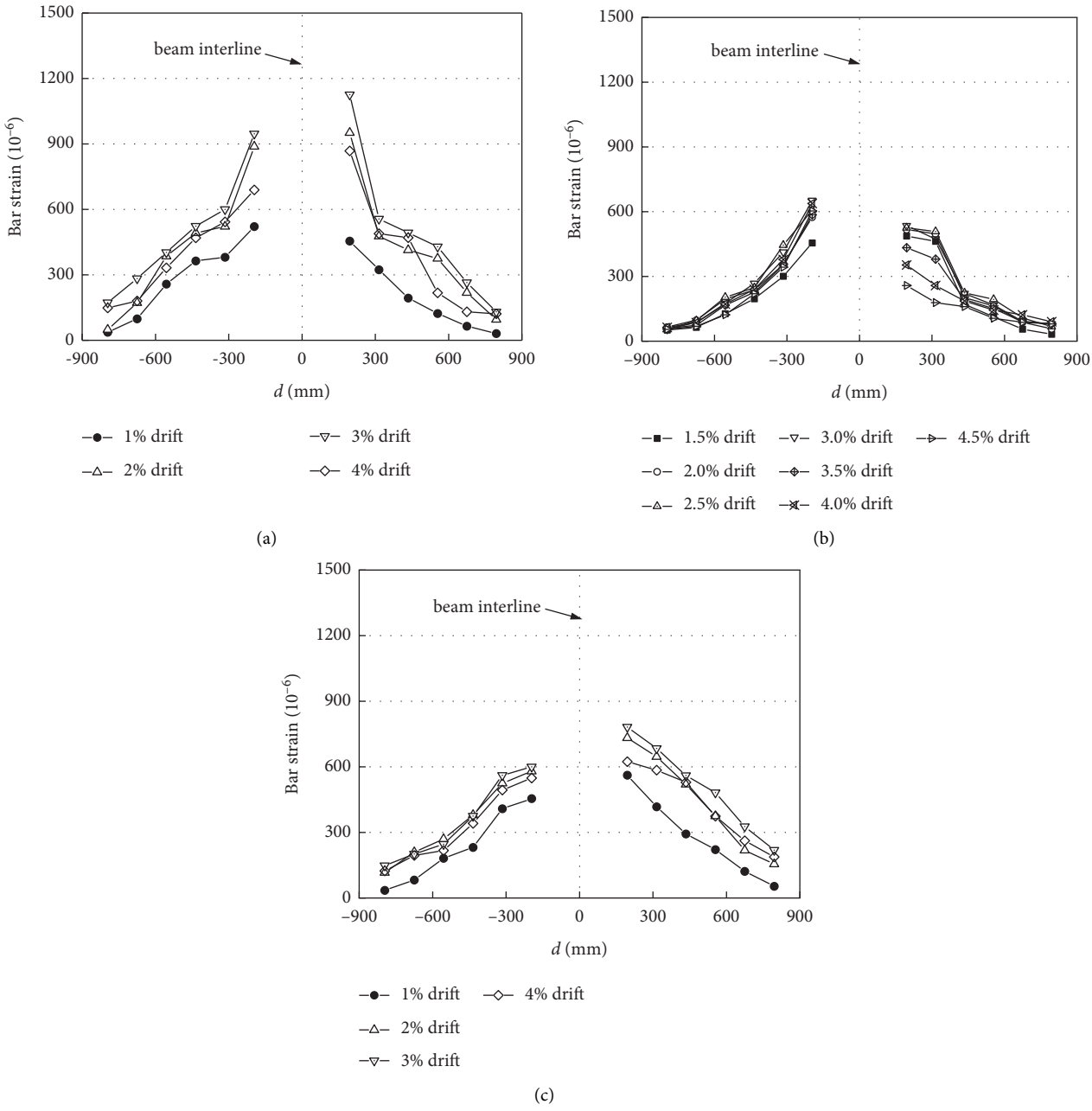

Figure 7: Strain variation of slab top reinforcement. (a) EBCSJ1. (b) EBCSJ2. (c) EBCSJ3.

Figure 8: Crack patterns in the beam-column intersection zone and slab. (a) EBCSJ1. (b) EBCSJ2. (c) EBCSJ3.

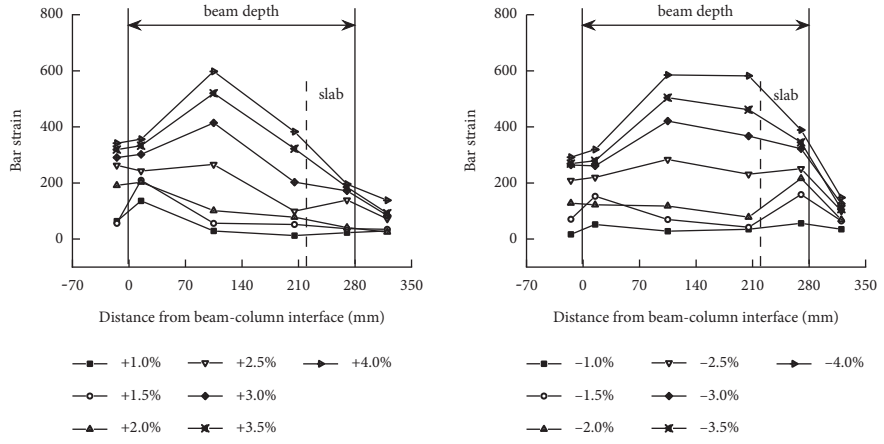

(a)

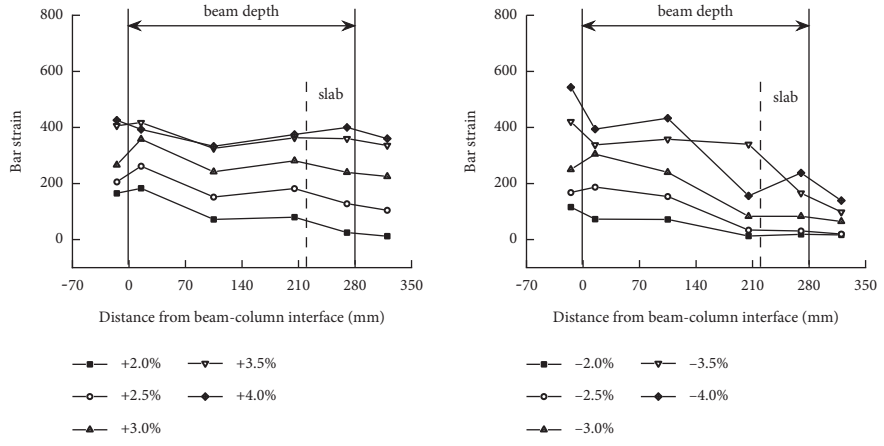

(b)

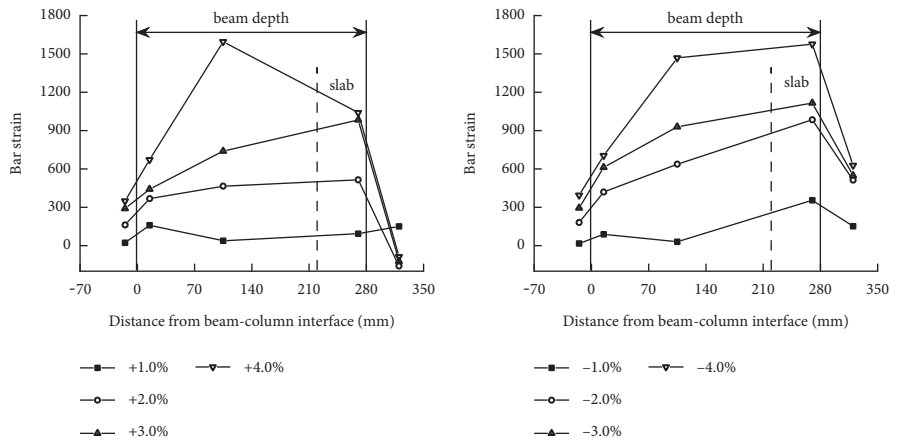

(c)

Figure 9: Continued.

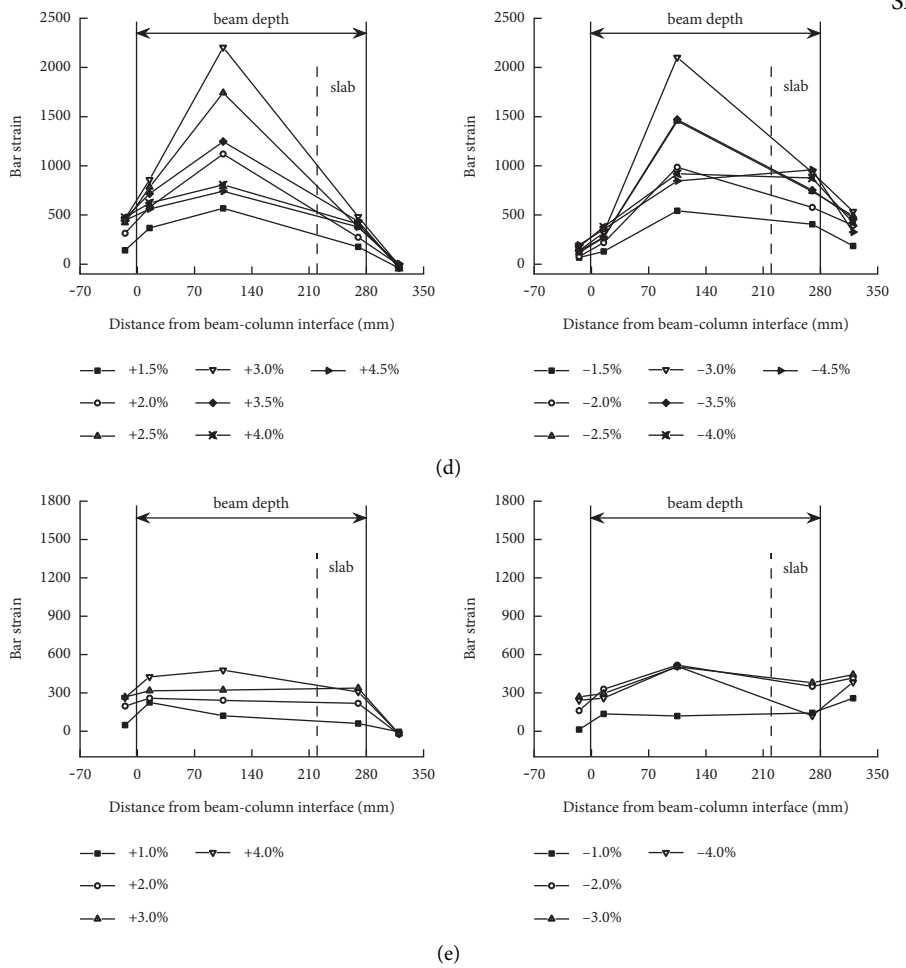

Figure 9: Strain variation of hoop near core. (a) EBCJ1. (b) EBCJ2. (c) EBCSJ1. (d) EBCSJ2. (e) EBCSJ3.

area of each specimen along the height of the frame beam section is shown in Figure 9.

It can be seen from Figure 9 that the strain of stirrups near the core area (including the top of the column and the foot of the column) is in good agreement with the experimental phenomenon. (a) The plane specimens EBCJ1 and EBCJ2 did not suffer from shear failure in the core area. Therefore, the strain of the stirrups in the core area did not yield, and under the same displacement angle, the strain of specimen EBCJ2 with a large strong column coefficient was slightly smaller. (b) Specimens EBCSJ1 and EBCSJ2 with slabs form weak joints due to the participation of the cast-in-place plates. As a result, the stirrups in the core region were close to yielding, especially the core region of the specimen EBCSJ2 that was about to fail (its bond properties also started to degrade earlier). Compared with the comparison specimen EBCSJ1, the peak value of stirrup strain in the core area of specimen EBCSJ3 is significantly reduced, which is equivalent to that of the flat specimen EBCJ1, and the mechanical performance is better.

3.5. Energy Dissipation. Figure 10 shows the hysteretic energy dissipation curves of different beam-column joints under different loading grades. As can be seen from the figure, specimens in the small deformation stage have less energy dissipation. For displacement values below 10 mm, the specimens dissipate almost the same amount of energy. Between 10 mm and 40 mm, the EBCSJ3 specimen dissipates a larger amount of energy than the other specimens do. Beyond 40 mm, EBCJ2 specimen dissipates larger and larger amounts of energy approximately double that of EBCJ1 specimen at a displacement of 50 mm. Until the displacement is equal to 40 mm, EBCJ1 and EBCJ2 specimens show practically the same dissipation capacity. Beyond displacement = 40 mm, the effect owing to the larger shear force prevails, and therefore, the EBCSJ3 specimen dissipates a larger amount of energy with respect to the EBCJ2 specimen.

The energy dissipation of joints increases with increasing column-to-beam flexural strength. Under the same axial compression ratio, the reinforcement of the column can slightly improve the energy consumption. In comparing the five specimens, the specimens without the slab have better energy dissipation ability than the specimens with the slab. This may be caused by the slab increasing beam resistance in tension and compression and reducing the column-to-beam flexural strength.

The viscous damping ratio is often adopted to normalize the dissipated energy [34, 35]. This ratio of all the specimens at different displacement levels is shown in Figure 11. When the peak load reached, the viscous damping ratio of specimens EBCJ2 and EBCSJ1 was 0.09, and that of specimens EBCJ1 and EBCJ3 was similar, about 0.11, which increased by 22.2%.

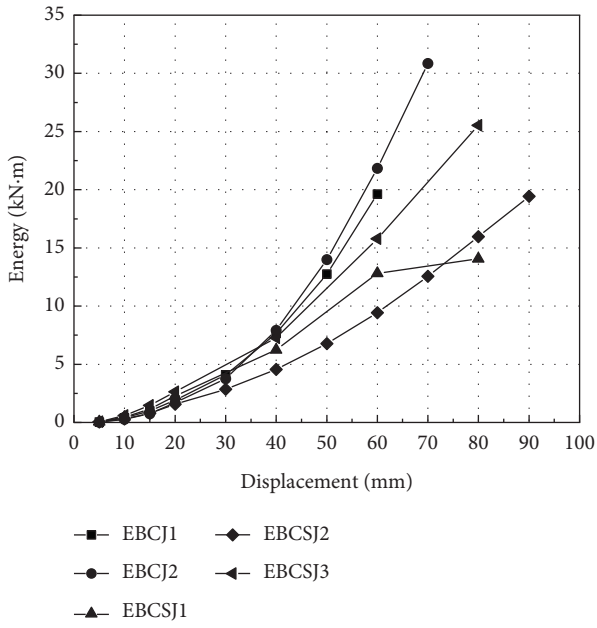

Figure 10: Energy dissipation of joint specimens.

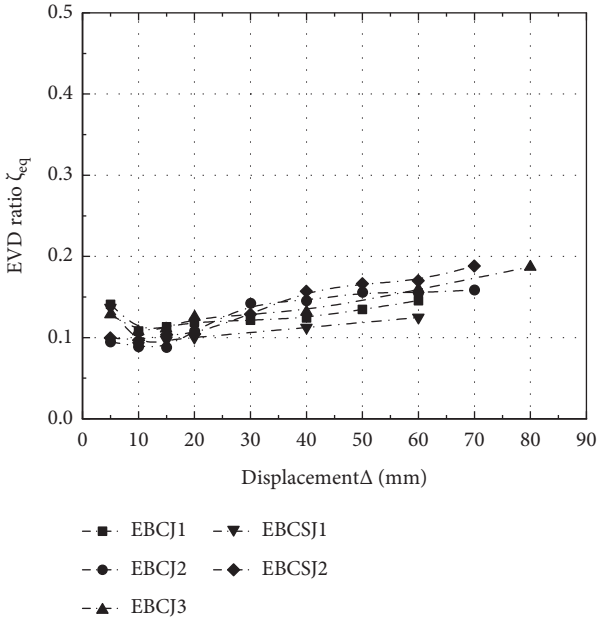

Figure 11: Viscous damping ratio.

When the specimen failed, the viscous damping ratios of specimens EBCJ1, EBCJ2, EBCJ3, EBCSJ1, and EBCSJ2 are 0.146, 0.159, 0.187, 0.125, and 0.188, respectively.

4. Finite Element Simulation

To numerically study the seismic performance and failure mechanism of the joint specimens, a 3D finite element (FE) simulation was performed using ABAQUS 6.14 [36]. In this study, a FE model that can be used to simulate and predict the seismic response of the joints with or without slab was established. The feasibility and accuracy of the proposed mode were validated by comparing the results between experiment and the numerical simulation.

4.1. Material Modeling. Usually, there are three different approaches including the smeared cracking mode, brittle cracking mode, and concrete damage plasticity (CDP) model available in the FE software ABAQUS 6.14 [36] to simulate the concrete behavior. In this study, the CDP mode was employed, which was first proposed by Lubliner et al. [37] and improved by Lee and Fenves [38].

In the CDP model, several critical parameters are needed to define the performance of concrete under triaxial stress, and the default values of these parameters recommended by ABAQUS were selected in the present analysis. The parameters include (1) the dilation angle ($\psi = 30^{\circ}$); (2) the flow potential eccentricity ($e = 0.1$); (3) the viscosity parameter ($\mu = 0.005$); and (4) the compressive strength ratio under biaxial loading to that under uniaxial loading ($f_{b0}/f_c' = 1.16$). Other parameters take the system default value.

In addition to the parameters, the stress-strain relationships of concrete under tension and compression are also required. According to the constitutive relation proposed in the Chinese code for the design of concrete structures (GB510010-2010) [32], the stress-strain curves of concrete under compression and tension are selected. The following equations show the nonlinear stress-strain relation of concrete in compression and tensile, respectively:

$$\sigma = \begin{cases} f_c \left[\alpha_a \dfrac{\varepsilon}{\varepsilon_p} + (3 - 2\alpha_a)\left(\dfrac{\varepsilon}{\varepsilon_p}\right) + (\alpha_a - 2)\left(\dfrac{\varepsilon}{\varepsilon_p}\right)^3 \right], & \varepsilon < \varepsilon_p, \\ f_c \left[\dfrac{\varepsilon}{\varepsilon_p \alpha_d \left(\varepsilon/\varepsilon_p - 1\right)^2 + \varepsilon} \right], & \varepsilon \geq \varepsilon_p. \end{cases} \tag{1}$$

$$\sigma_t = f_t \frac{\varepsilon_t}{\varepsilon_{tp} \alpha_t \left(\varepsilon_t/\varepsilon_{tp} - 1\right)^{1.7} + \varepsilon_t/\varepsilon_{tp}^2}, \varepsilon_t \geq \varepsilon_{tp}, \tag{2}$$

where f_c is the compressive strength of concrete; f_t is the tensile strength of the concrete; ε_c is the uniaxial compressive strain of concrete; ε_t is the tensile strain of the concrete; σ_c is the stresses corresponding to the strain ε_c; σ_t is the stresses corresponding to the strain ε_t; ε_p is 0.002 [39] for the corresponding strain of concrete compressive strength; and α_a and α_d are 1.78 and 2.48, respectively, which indicate the rising and falling parts of the stress-strain curve of concrete under uniaxial compression and tensile loading.

The behavior of steel material was assumed as an elastic-plastic segment with isotropic strain hardening and identical behavior in tension and compression, and the values of the parameters that describe the stress-strain curve of steel material for different bar diameters were obtained from the experimental part of this study, as presented in Table 2.

4.2. Element Types. Regarding the different material properties of the concrete and steel rebars, the two materials were modeled separately with different element types. An 8-node trilinear element (C3D8R) was used to simulate the

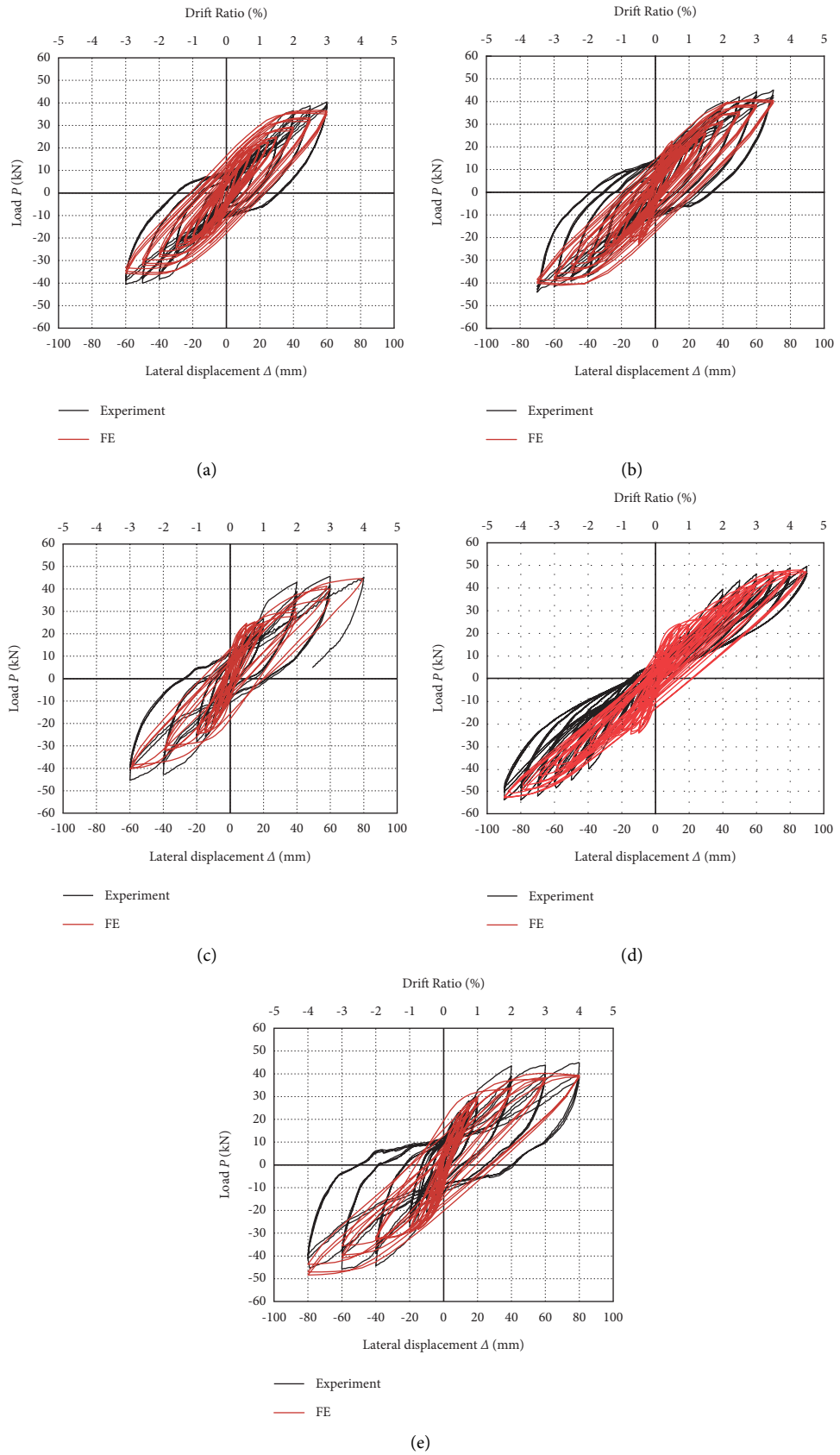

Figure 12: Comparison between numerical and test results. (a) EBCJ1. (b) EBCJ2. (c) EBCSJ1. (d) EBCSJ2. (e) EBCSJ3.

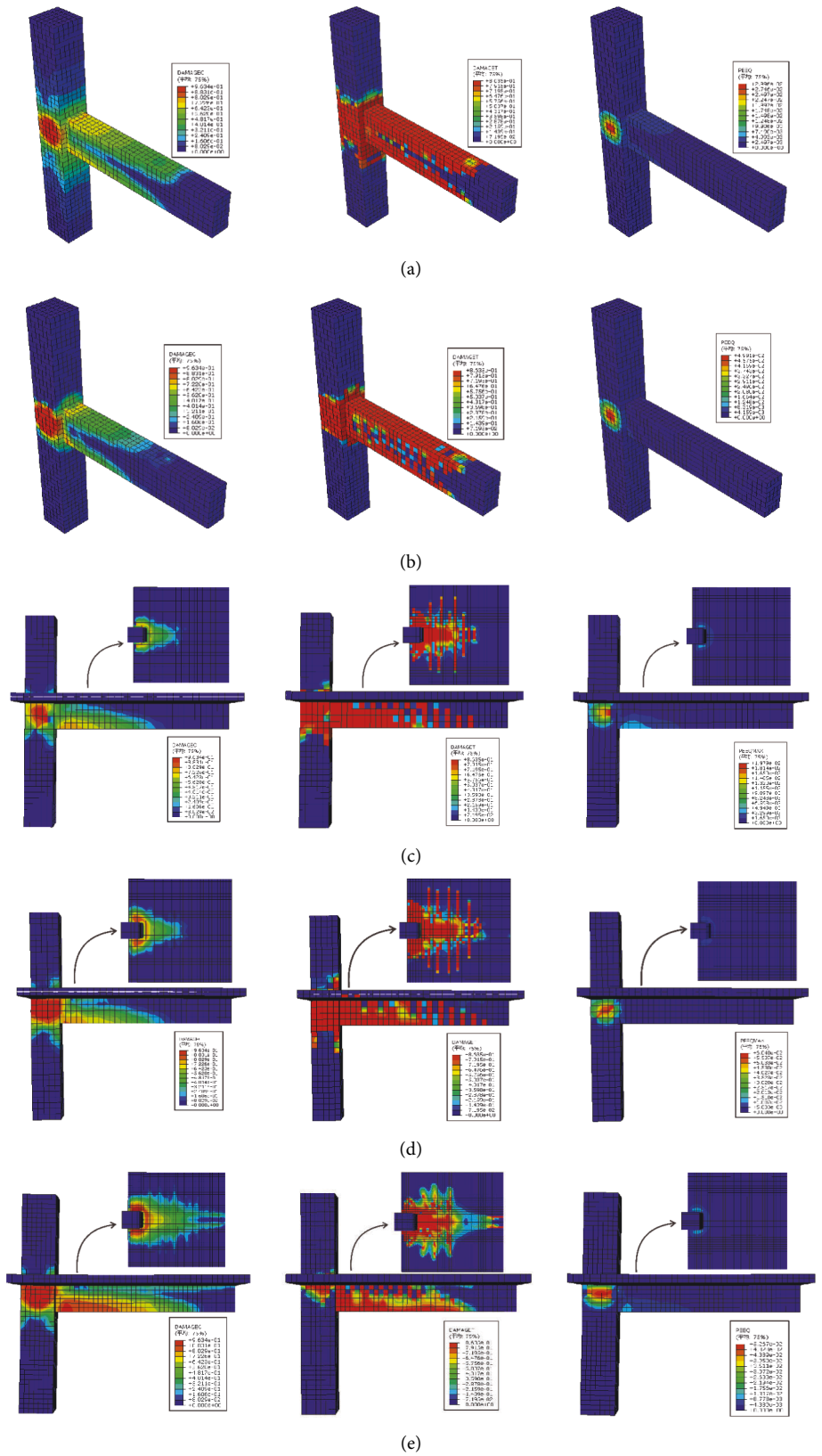

(a)

(b)

(c)

(d)

(e)

Figure 13: FEA outputs of the exterior beam-column joints at yield force of shear behavior. (a) EBCJ1. (b) EBCJ2. (c) EBCSJ1. (d) EBCSJ2. (e) EBCSJ3.

nonlinear behavior of concrete, since the element contains three translational degrees and could simulate the tensile cracking and compression crushing ability. For steel, the truss element (T3D2) was adopted to model its behavior [40]. Furthermore, the steel rebars were inserted into the concrete with an embedded technique, provided by ABAQUS 6.14 [36] employed to model the interaction between the concrete and steel rebars. This means that the reinforcements are completely bonded to the surrounding concrete, and there will be no slippage in the interaction between the concrete and the reinforcement.

4.3. Loading and Boundary Conditions. Two different approaches can be used to operate the finite element analysis in the ABAQUS software [31], including displacement control system and force control system. In this study, the displacement control approach was used because it can overcome the convergence problem and be able to the monitor the behavior of simulated joints after reaching the maximum load. Based on the test setup and loading system described in second section, appropriate restraints were utilized to simulate the test conditions.

4.4. Finite Element Analysis Results. Figure 12 shows the experimental and numerical results regarding the load-lateral displacement relationship for all the exterior beam-column joint specimens. Comparing the behavior of the specimens, the FE analysis showed generally slightly higher initial stiffness than the test results. Differences can be found between the two results for all specimens, such as the shape of the hysteresis loop and the degradation of carrying capacity due to repeated cycles at a certain displacement. Fortunately, the maximum bearing capacities of the specimens obtained in the test and the simulation analysis were almost the same. The difference between the two results may be due to many factors including the effects of some hypothetical variables such as the selection properties of concrete (tensile and compressive) and the interaction property between the concrete and steel reinforcements, as well as the different loading systems caused by the possible material defects and differences in the experimental efforts.

Figure 13 presents the damage of concrete in the exterior beam-column joints under repeated cyclic lateral loading from FE simulation. DAMAGEC is the compressive damage of concrete, and DAMAGET is the tensile damage of concrete. PEEQ is the accumulated equivalent plastic strain.

In terms of the tensile damage, it can be seen from Figure 13 that the concrete tensile damage in joint specimens EBCJ1 and EBCJ2 is mainly located within core joints and the upper and lower parts of front view of the beams, while for the specimens with slabs, the tensile damage no longer appeared in the upper part of the beam, but in the interface area between the beams and the slabs adjacent to the column surface. Also, the core joints were the location where the maximum tensile damage occurred. As for the compressive damage, a similar situation could be observed with the tensile damage, except for the bigger regions, the slabs were covered in compression damage. The accumulated equivalent plastic strain was mainly formed in the joint core area. The addition of slabs seemed to have little effect on this characterization.

In addition, from Figure 13, the yield of longitudinal bars can be clearly observed, as well as tensile damage and compressive damage in the core joints. In the experiment, the concrete cracking develops to the joint area, then the longitudinal reinforcement of the beam yields, and the concrete crushing was found at the core joints. The results show that the phenomenon is consistent with the experimental results. Also, it could be found from the figure that the FE models had experienced a shear failure of core joint and flexural failure of the beam end. This is in consistence with the observation from the experimental results. Because the strength of stirrup and concrete was utilized sufficiently during the loading process, the seismic capacity of eccentric joints damaged by both bending and shearing is better than that of common joints that failed by bending only. The results demonstrate that the FE outcomes were in good agreement with the experimental results regarding the failure mode, which verifies the feasibility and accuracy of the model employed in this study.

5. Conclusion

The study presented experimental and numerical investigation on the seismic performance of five RC exterior beam-column joints with or without slabs. The effects of the slab and the beam-column moment strength ratio on the seismic behavior in terms of the failure modes, load-displacement hysteretic curves, shear response, and energy dissipation capacity were discussed. In addition, the results obtained from the numerical simulation and the laboratory experiment were compared. According to the analysis results, the conclusion can be concluded as follows:

(1) The damages of the exterior beam-column joints without slabs under repeated cyclic loading were concentrated on the upper and lower parts of the beam near the column, with sparse and diagonal cracks distributed in the joint area, while the damages to the three specimens with slabs occurred in the lower part of beams and the beam-column-slab interface, with dense and wider distribution of diagonal shear cracks in the joint region. The crack patterns and failure modes observed from the five joint specimens indicated that the joint shear transfer mechanisms were significantly affected by the slabs and flexural strength ratio of column to beam, as well as the loading system.

(2) In specimens EBCJ1 and EBCJ2, the core of the joint did not fail; however, the samples themselves were damaged owing to concrete crushing at the bottom of the beam end, and EBCJ2 develops a full-width plastic hinge on the beam. Specimens EBCSJ1 and EBCSJ2 failed in the interface between beam and column with concrete crushing, whereas specimen EBCSJ3 failed in the beam-column interface with slab torsional failure. The results showed that the slab

had a significant influence on the failure mode of joints.

(3) Under the same axial compression ratio in experiment, the results showed that the energy dissipation capacities of the joint specimens increased with the flexural strength ratio of column to beam. The specimens without the slabs have better energy dissipation ability than the specimens with the slab due to the effect of slab for increasing beam resistance and reducing the flexural strength of column to beam.

(4) The specimens with slabs exhibited higher load carrying capacity than the specimens without slabs. However, the increased beam strength resulting from the slab effect may cause greater demands on the column, this harms the RC joint aswell as the RC frame structure as it could increase the possibility of shear failure of column or compression failure in the column if it is not considered properly.

(5) The seismic performance of the exterior beam-column joints with or without slabs was simulated by finite element analysis. The numerical results were compared with the experimental results to verify the effectiveness of the finite element models. Furthermore, the model provides an effective and powerful numerical tool for further study of different types of RC beam-column joints, as well as the joint with various design parameters.

Data Availability

The data used to support the findings of this study are available from the corresponding author upon request.

Conflicts of Interest

The authors declare no conflicts of interest.

Acknowledgments

The authors gratefully acknowledge the financial support from the Fundamental Research Funds for the Central Universities, CHD (No. 300102281303).

References

[1] B. Zhao, F. Taucer, and T. Rossetto, "Field investigation on the performance of building structures during the 12 May 2008 Wenchuan earthquake in China," *Engineering Structures*, vol. 31, no. 8, pp. 1707–1723, 2009.

[2] H. Y. Chang and K. C. Lin, "Reconnaissance observations on the buildings damaged by the 2010 Taiwan Kaohsiung earthquake," *Natural Hazards*, vol. 69, no. 1, pp. 237–249, 2013.

[3] G. Dogan, A. S. Ecemis, S. Z. Korkmaz, M. H. Arslan, and H. H. Korkmaz, "Buildings damages after elazığ, Turkey earthquake on january 24, 2020," *Natural Hazards*, vol. 109, no. 1, pp. 161–200, 2020.

[4] L. Hung-Jen and K. Jen-Wen, "Eccentric reinforced concrete beam-column connections subjected to cyclic loading in principal directions," *ACI Structural Journal*, vol. 104, no. 4, p. 459, 2007.

[5] A. Masi, G. Santarsiero, G. P. Lignola, and G. M. Verderame, "Study of the seismic behavior of external RC beam-column joints through experimental tests and numerical simulations," *Engineering Structures*, vol. 52, no. 6, pp. 207–219, 2013.

[6] M. N. Kataoka, M. A. Ferreira, and A. L. H. de Cresce El Debs, "Nonlinear FE analysis of slab-beam-column connection in precast concrete structures," *Engineering Structures*, vol. 143, no. 7, pp. 306–315, 2017.

[7] H. Behnam and J. S. Kuang, "Exterior RC wide beam-column connections: effect of spandrel beam on seismic behavior," *Journal of Structural Engineering*, vol. 144, no. 4, Article ID 04018013, 2018.

[8] F. Gao, Z. Tang, S. Mei, B. Hu, S. Huang, and J. Chen, "Seismic behavior of exterior beam-column joints with high-performance steel rebar: experimental and numerical investigations," *Advances in Structural Engineering*, vol. 24, no. 1, pp. 90–106, 2021.

[9] M. A. Najafgholipour and A. R. Arabi, "A nonlinear model to apply beam-column joint shear failure in analysis of RC moment resisting frames," *Structures*, vol. 22, no. 9, pp. 13–27, 2019.

[10] B. Hu and T. Kundu, "Seismic performance of interior and exterior beam–column joints in recycled aggregate concrete frames," *Journal of Structural Engineering*, vol. 145, no. 3, Article ID 04018262, 2019.

[11] P. Chetchotisak, E. Arjsri, and J. Teerawong, "Strut-and-tie model for shear strength prediction of RC exterior beam–column joints under seismic loading," *Bulletin of Earthquake Engineering*, vol. 18, no. 4, pp. 1525–1546, 2020.

[12] S. Alavi-Dehkordi, D. Mostofinejad, and P. Alaee, "Effects of high-strength reinforcing bars and concrete on seismic behavior of RC beam-column joints," *Engineering Structures*, vol. 183, no. 7, pp. 702–719, 2019.

[13] G. M. S. Alva, A. L. H. de Cresce El Debs, and M. K. El Debs, "An experimental study on cyclic behaviour of reinforced concrete connections," *Canadian Journal of Civil Engineering*, vol. 34, no. 4, pp. 565–575, 2007.

[14] S. Sasmal, K. Ramanjaneyulu, B. Novák, and N. Lakshmanan, "Analytical and experimental investigations on seismic performance of exterior beam-column subassemblages of existing RC-framed building," *Earthquake Engineering & Structural Dynamics*, vol. 42, no. 12, pp. 1785–1805, 2013.

[15] C. Marthong, A. Dutta, and S. K. Deb, "Effect of cyclic loading frequency on the behavior of external RC beam-column connections," *Journal of Earthquake Engineering*, vol. 20, no. 7, pp. 1126–1147, 2016.

[16] C. G. Karayannis and E. Golias, "Full-scale experimental testing of RC beam-column joints strengthened using CFRP ropes as external reinforcement," *Engineering Structures*, vol. 250, no. 2, Article ID 113305, 2022.

[17] C. Karayannis, E. Golias, and G. I. Kalogeropoulos, "Influence of carbon fiber-reinforced ropes applied as external diagonal reinforcement on the shear deformation of RC joints," *Fibers*, vol. 10, no. 3, 2022.

[18] R. Leon and J. O. Jirsa, "Bidirectional loading of R.C. Beam-column joints," *Earthquake Spectra*, vol. 2, no. 3, pp. 537–564, 1986.

[19] A. J. DurraniI and J. K. Wight, "Earthquake resistance of reinforced concrete interior connections including a floor slab," *Structural Journal*, vol. 84, no. 5, pp. 400–406, 1987.

[20] G. Santarsiero and A. Masi, "Analysis of slab action on the seismic behavior of external RC beam-column joints," *Journal of Building Engineering*, vol. 32, no. 6, Article ID 101608, 2020.
[21] C. Ma, Z. Wang, and S. T. Smith, "Seismic performance of large-scale RC eccentric corner beam-column-slab joints strengthened with CFRP systems," *Journal of Composites for Construction*, vol. 24, no. 2, Article ID 04019066, 2020.
[22] W. Y. Kam, P. Quintana Gallo, U. Akguzel, and S. Pampanin, "Influence of slab on the seismic response of sub-standard detailed exterior reinforced concrete beam column joints," in *Proceedings of the 9th US National and 10th Canadian Conference on Earthquake Engineering: Reaching beyond Borders*, Toronto, Canada, July 2010.
[23] S. Park and K. M. Mosalam, "Experimental investigation of nonductile RC corner beam-column joints with floor slabs," *Journal of Structural Engineering*, vol. 139, no. 1, pp. 1–14, 2013.
[24] C. W. French and J. P. Moehle, "Effect of floor slab on behavior of slab-beam-column connections, " ACI," *Special Publication*, vol. 123, no. 9, pp. 225–258, 1991.
[25] P. C. Cheung, T. Paulay, and R. Park, "Mechanisms of slab contributions in beam-column subassemblages," *ACI Special Publications*, vol. 123, no. 8, pp. 259–290, 1991.
[26] J. M. LaFave and J. K. Wight, "Reinforced concrete exterior wide beam-column-slab connections subjected to lateral earthquake loading," *Structural Journal*, vol. 96, no. 4, pp. 577–585, 1999.
[27] S. J. Pantazopoulou and C. W. French, "Slab participation in practical earthquake design of reinforced concrete frames," *Structural Journal*, vol. 98, no. 4, pp. 479–489, 2001.
[28] M. Shin and J. M. LaFave, "Reinforced concrete edge beam-column-slab connections subjected to earthquake loading," *Magazine of Concrete Research*, vol. 56, no. 5, pp. 273–291, 2004.
[29] S. M. Ahmed, C. Umarani, and G. A. MacRae, "A parametric study of RC slab in beam-column connection under cyclic loading," in *Proceedings of the New Zealand Society for Earthquake Engineering Conference*, Christchurch, New Zealand, April 2012.
[30] S. Chen, W. Yan, and J. Gao, "Experimental investigation on the seismic performance of large-scale interior beam-column joints with composite slab," *Advances in Structural Engineering*, vol. 15, no. 7, pp. 1227–1237, 2012.
[31] G. H. Xing, C. Zhou, T. Wu, and B. Q. Liu, "Effective flange width of cast-in-situ slab under tension for reinforced concrete exterior joints," *Journal Building Structural*, vol. 38, no. 8, pp. 65–73, 2017.
[32] Cina Ministry of Construction of the People, *Code for Seismic Design of Buildings*, China Building Industry Press, Beijing, China, 2010.
[33] China Architecture and Building Press, *Development of the People's Republic of China: Specification for Seismic Test of Buildings (JGJ/T 101-2015)*Ministry of Housing and Urban-Rural, Chinese, 2015.
[34] C. G. Karayannis and E. Golias, "Full scale tests of RC joints with minor to moderate seismic damage repaired using C-FRP sheets," *Earthquakes and Structures*, vol. 15, no. 6, pp. 617–627, 2018.
[35] G. M. Verderame, M. T. De Risi, and P. Ricci, "Experimental investigation of exterior unreinforced beam-column joints with plain and deformed bars," *Journal of Earthquake Engineering*, vol. 22, no. 3, pp. 404–434, 2018.
[36] Simulia, *Abaqus User's Manual Version 6.14*, Dassault Systemes Simulia Corp, Providence, Rhode Island, USA, 2014.
[37] J. Lubliner, J. Oliver, S. Oller, and E. Onate, "A plastic-damage model for concrete," *International Journal of Solids and Structures*, vol. 25, no. 3, pp. 299–326, 1989.
[38] J. Lee and G. L. Fenves, "Plastic-damage model for cyclic loading of concrete structures," *Journal of Engineering Mechanics*, vol. 124, no. 8, pp. 892–900, 1998.
[39] X. M. Zhao, Y. F. Wu, and A. Y. T. Leung, "Analyses of plastic hinge regions in reinforced concrete beams under monotonic loading," *Engineering Structures*, vol. 34, no. 9, pp. 466–482, 2012.
[40] X. J. Zhou, X. Y. Kou, Q. M. Peng, and J. T. Cui, "Influence of infill wall configuration on failure modes of RC frames," *Shock and Vibration*, vol. 2018, no. 9, pp. 1–14, 2018.